2007

Geometrical modeling of fibrous materials under compression

Benoit Maze
NC State University

Hooman Vahedi Tafreshi
Virginia Commonwealth University, htafreshi@vcu.edu

Behnam Pourdeyhimi
NC State University

Geometrical modeling of fibrous materials under compression

Benoit Maze
Nonwovens Cooperative Research Center, NC State University, Raleigh, North Carolina 27695-8301, USA

Hooman Vahedi Tafreshi[a)]
Mechanical Engineering Department, Virginia Commonwealth University, Richmond, Virginia 23284-3015, USA

Behnam Pourdeyhimi
Nonwovens Cooperative Research Center, NC State University, Raleigh, North Carolina 27695-8301, USA

Many fibrous materials such as nonwovens are consolidated via compaction rolls in a so-called calendering process. Hot rolls compress the fiber assembly and cause fiber-to-fiber bonding resulting in a strong yet porous structure. In this paper, we describe an algorithm for generating three dimensional virtual fiberwebs and simulating the geometrical changes that happen to the structure during the calendering process. Fibers are assumed to be continuous filaments with square cross sections lying randomly in the *x* or *y* direction. The fibers are assumed to be flexible to allow bending over one another during the compression process. Lateral displacement is not allowed during the compaction process. The algorithm also does not allow the fibers to interpenetrate or elongate and so the mass of the fibers is conserved. Bending of the fibers is modeled either by considering a constant "slope of bending" or constant "span of bending." The influence of the bending parameters on the propagation of compression through the material's thickness is discussed. In agreement with our experimental observations, it was found that the average solid volume fraction profile across the thickness becomes U shaped after the calendering. The application of these virtual structures in studying transport phenomena in fibrous materials is also demonstrated. © *2007 American Institute of Physics*. [DOI: 10.1063/1.2794476]

I. INTRODUCTION

In manufacturing nonwovens, thermoplastic fibers are often bonded together by thermal calendering (see Fig. 1). In this process, the calender rolls slightly melt the surface of the fibers and cause them to fuse together at the crossovers. Hot calendering causes permanent changes in the structure and depending on the temperatures and pressures used in the process, various degrees of densification and fiber linkage can be achieved.

During the past years, there have been many pioneering works aimed at simulating the three dimensional (3D) structure of a fibrous material. Qi and Uesaka[1] generated 3D anisotropic virtual media made of interpenetrating fibers to model paper boards. With the same objective but in a different way, Koponen *et al.*[2] modeled 3D structures made up of short fibers based on a model developed by Niskanen and Alava.[3] Further investigations on 3D assembly of interpenetrating fibers have been conducted by Clague and Phillips[4] and Tomadakis and Robertson[5] who investigated the permeability of their fibrous media. In all the above studies, once a fibrous medium was generated, no further processing was performed on it. Thus, these studies have been limited to uncompressed assemblies of (discontinuous) fibers. Note that there are a few available published works dealing with compressing fibrous materials. These studies, however, are focused on stiffness and rigidity of fibrous materials (Kello-

maki *et al.*,[6] Astrom *et al.*,[7] and Wu and Dzenis[8]). Our objective in this paper, however, is to simulate the structure of a nonwoven material before and after calendering. Since our fibers are continuous, these nonwovens would be similar to those produced by spun bonding. Spun bonding is a manufacturing technology which offers a one-step process for producing nonwovens from the raw materials (thermoplastic polymers) as the fiber and fabric productions are combined. Spun bonded fibers are continuous filaments that are quenched and drawn to form highly oriented crystalline fiber morphologies. Once collected in a web form, the fibers need to be bonded to form a fabric. Calendering is a common process used for thermally bonding spun bonded webs. In the current paper, we generate virtual spun bonded nonwovens and simulate the changes in their microstructural geometry
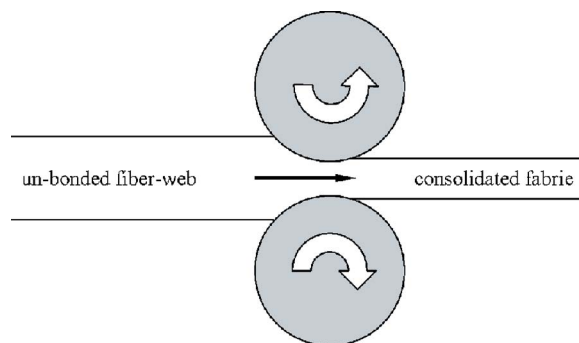

FIG. 1. (Color online) A schematic drawing of smooth calender bonding. Drawing is not to scale.

a)Author to whom correspondence should be addressed. Tel.: 804-828-9936. FAX: 804-827-7030. Electronic mail: htafreshi@vcu.edu
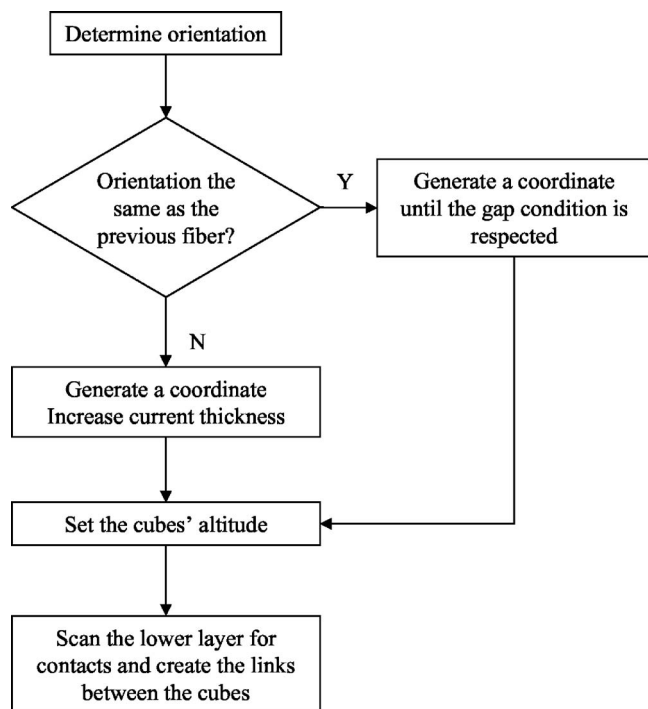
FIG. 2. The flowchart of the procedure developed for generating uncompressed webs.

FIG. 3. (Color online) An example of the uncompressed webs generated by our algorithm.

during the calendering process at different compaction ratios (the ratio of the original to final thicknesses). The next section will describe our algorithm for generating spun bonded nonwovens. This will be followed by a section on virtually compressing these media in Sec. III. The application of the current geometric modeling in calculating transport phenomena in fibrous materials is briefly discussed in Sec. IV followed by the conclusions in Sec. V.

II. GENERATING UNCOMPRESSED FIBERWEBS

Most nonwovens can be assumed to be 3D layered structures. Such structures consist of a large number of fibers or filaments sequentially deposited on top of one another in a somewhat random manner in a horizontal plane to build the required 3D geometry. Consequently, there is a great difference between their properties in the in-plane and through-plane directions. As mentioned before, there are a few available published studies attempting to generate 3D fibrous structures, but in most of these works, fibers were assumed to interpenetrate into each other at the crossovers, which obviously is unrealistic.[4,5,9,10] Here, we plan to construct the above-mentioned 3D structure of stacked horizontal fibers with no volume (mass) loss. In order to simulate a spun bonded nonwoven web suitable for compaction, we considered the fibers to have square cross sections and lie horizontally in the plane of the web and only in the x or y direction unlike our previous web generation algorithm.[11–13] This will ease the fiber bending process as will be explained later in the next section. The fibers are represented by a succession of cubes of size 1, with integer coordinates in the x and y directions. This also means that all the dimensions are non-dimensionalized by the fiber diameter.
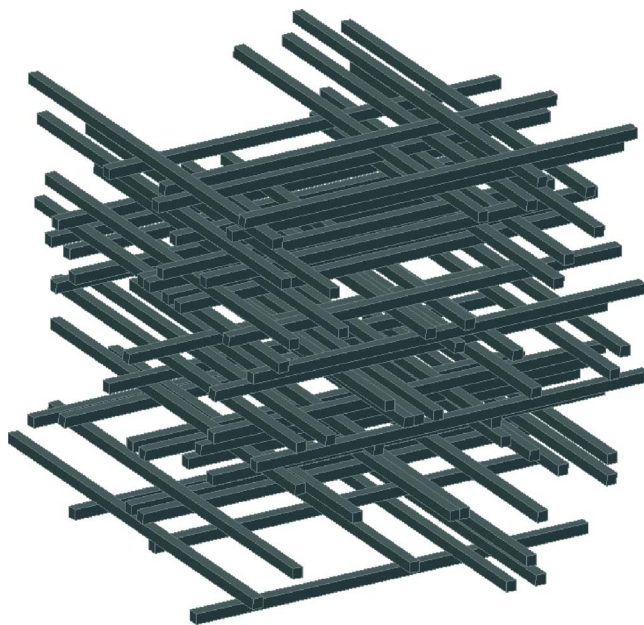
To generate an uncompressed 3D web, for each fiber, the first step is to determine the orientation. This orientation, being either in the x or y direction, is chosen randomly but according to a given proportion. This allows us to generate anisotropic fiberwebs where the number of fibers in the x direction, for instance, is greater than that in the y direction. If the orientation is the same as that of the previously generated fiber, the current altitude is kept constant as the fiber will be created in the current layer. Accordingly, if the orientation is different, the current altitude is increased and the fiber will be generated in a new layer. The next step consists in generating a coordinate for this fiber: as the fibers are of infinite length, a fiber which is oriented in the x direction only needs a y coordinate. In order to have control on the minimum distance between two parallel fibers, a gap parameter g is introduced. The cases of $g=0$ and $g=2$, for instance, correspond to the condition where the minimum spacing between two parallel fibers having identical height (z) is zero and two fiber diameters, respectively. Note that a case of $g=-1$ which represents the case of two parallel fibers deposited on top of each other is not allowed (see the flowchart in Fig. 2). Because of this gap parameter, tentative coordinates will be generated for the fiber until one fulfills the gap condition for all the fibers already present in that layer. If no coordinate can be found, the fiber orientation is changed.

The last stage, establishing contacts between the new fiber and the ones below it, is crucial for the compression part of the simulation. For that purpose, a cube being in contact with another cube from above or below contains references to the contacted cube and its hosting fiber. This will facilitate the propagation of bending.

The above fiber deposition process will be repeated until the targeted dimensionless basis weight or thickness is reached. We define the dimensionless basis weight as the ratio of the total volume (or weight) of the fibers to the surface area of the sample. We consider volume and weight
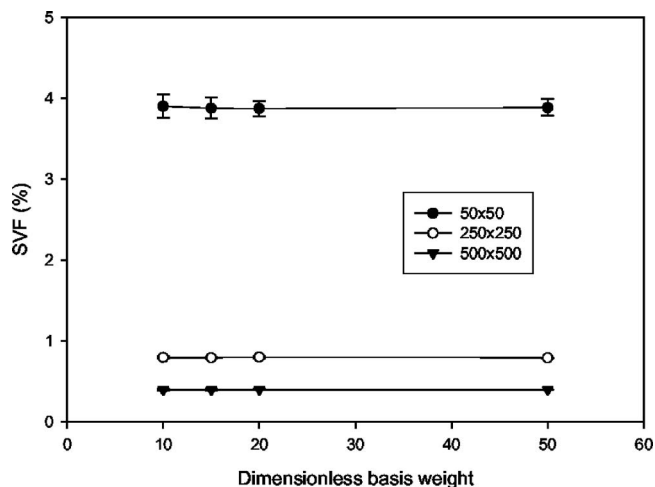
FIG. 4. SVF of the square samples with the side lengths of 50, 250, and 500 units having different dimensionless basis weights.

FIG. 6. Influence of fiber orientation distribution on SVF of the fiberweb.

to be interchangeable, i.e., we assume a density of 1 for the fibers. Note that the size of the sample and the length of the fibers are identical as the fibers are assumed to be continuous filaments. Therefore, dimensionless basis weight simply becomes the ratio of the number of fibers to the sample size.

Figure 3 shows a 50×50 web made of 80 fibers with a length of 50 spanning across the sample from isometric views. As mentioned before, spun bonded webs are made of continuous filaments collected and compacted together in the form of planar fibrous structures. The aforementioned web generation algorithm places the ends of each fiber at the peripheral boundaries of the square boxes considered for the simulations. In Fig. 4 we plotted the solid volume fraction (SVF) of square samples with the side lengths of 50, 250, and 500 units having different dimensionless basis weights (SVF is shown in percentile for convenience). It can be seen that the SVF of the webs made with this algorithm is independent of the basis weight. Note that this is what one may expect from any porous medium, i.e., increasing the thickness does not influence the solidity of the medium. Adding a larger number of fibers per unit of area simply increases the thickness of the web without changing its SVF. It can be seen
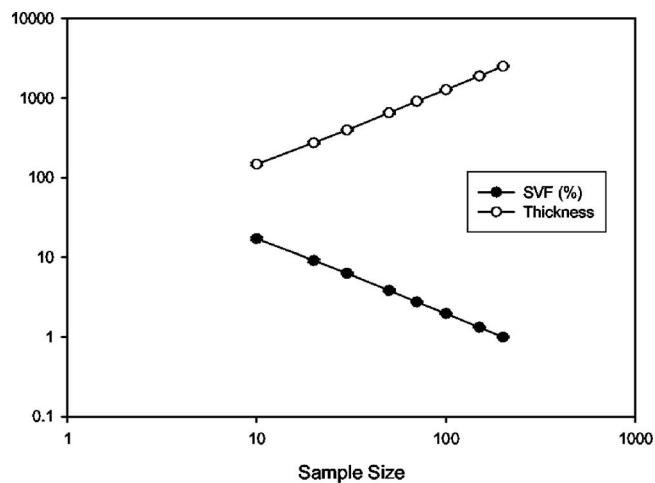
that SVF is only a function of the size of the sample being generated. Increasing the width of the box in our algorithm causes a reduction in the SVF. The SVF of a real nonwoven fiberweb is independent of the sample size as long as the sample size is sufficiently larger than the smallest length scale in the medium. Defining the length scale in fibrous media is difficult especially in the cases where fibers have no finite length such as spun bond filters. Spun bond filters are made of continuous filaments curled, coiled, and stacked on top of each other. It is a fact that such fiberwebs are made up of sequential depositions of these filament segments on top of each other. The diameter of these spiral trajectories is much larger than the size of the samples that one can produce in a regular personal computer with finite amount of accessible memory and computing speed. To this end, we modeled such structures with straight objects extending from one end of the sample to the other. This causes the SVF to become dependent on the sample size and one needs to use the relevant sample size to simulate a given nonwoven sheet. The origin of this counterintuitive property of our model is that on average, the number of fibers per layer is relatively independent of the sample size, whereas their length is not (i.e., the length of the fiber and size of the sample are the

FIG. 5. Influence of sample size on the web SVF and thickness at a fixed dimensionless basis weight.

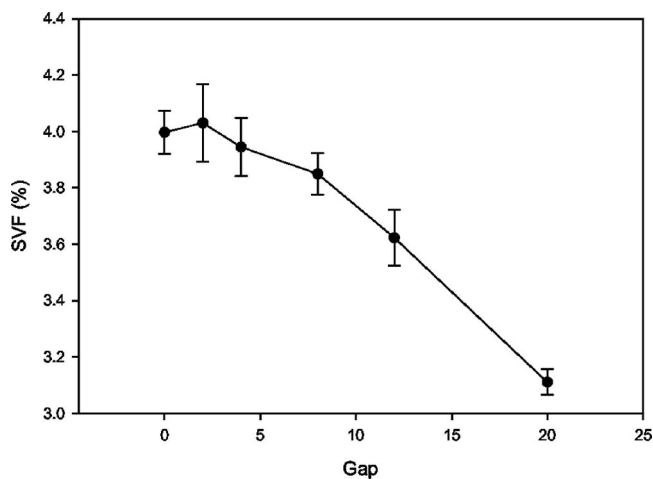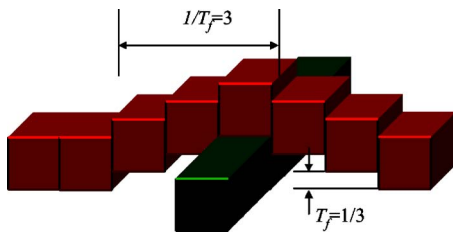FIG. 7. Influence of the gap size on SVF.

FIG. 8. (Color online) Fiber bending at crossovers.

same). As a consequence, when changing the sample size, the total volume of the fibers varies linearly while the volume of the whole fiberweb changes in proportion to the square of the sample size. Cutting subsamples from a 100 $\times$ 100 web, for instance, will result in media with lower SVFs unless the subsample size is greater than a critical size. The reason is that when one cuts a small subsample from a modeled large fiberweb, there will be some vertical gaps between the fibers in the subsample. These gaps are formed because some of the fibers in the subsample are deposited on fibers which are part of the large original web but are not in the subsample. Obviously, the smaller the subsample, the greater is the chance that fibers in the subsample have vertical gaps between them. However, if the subsample is larger than some critical size (a size comparable to that of the original sample), the subsample's SVF will be close to that of the original sample.

In order to find the sample size that can resemble a real spun bonded fabric of a given initial basis weight and SVF (before the compaction), we generated different spun bonded webs having an identical dimensionless basis weight in square boxes with different sizes (see Fig. 5). The rapid decrease in the SVF with increasing sample size is evident. Note that the thickness of the web increases by increasing the sample size for a fixed basis weight.

The uncalendered nonwovens discussed above were made up of an assembly of fibers laid down in either of the x or y direction with equal probabilities. Our algorithm allows generating fiberwebs in which fibers are deposited in the x or y direction but with unequal chances. The reason for this is that most of the fiberweb production processes introduce
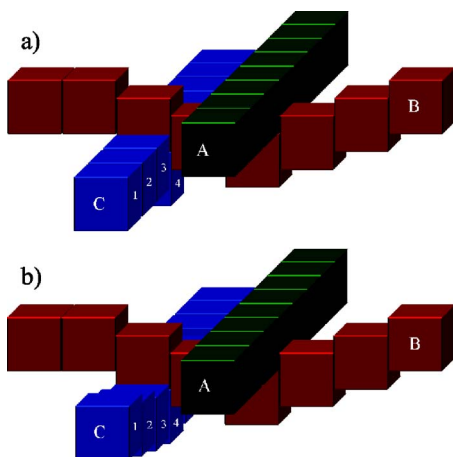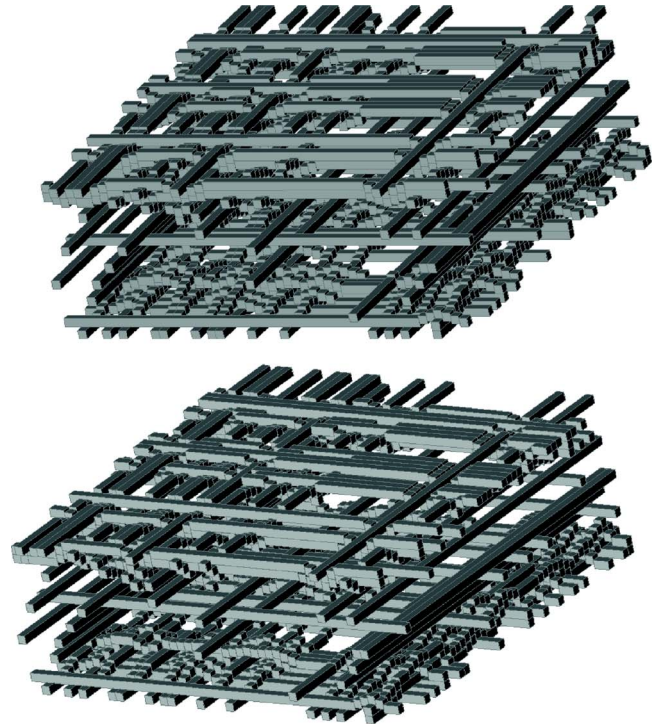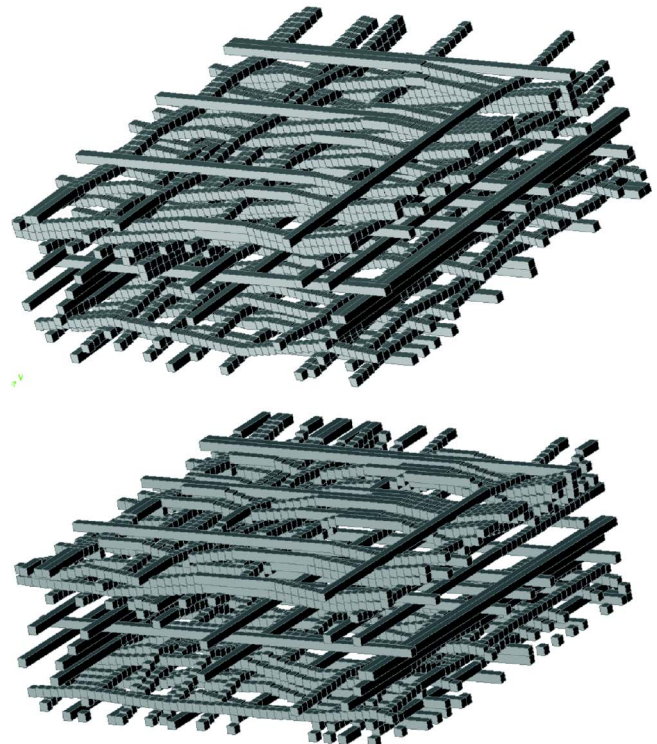
some degrees of directionality to the fiberwebs which can potentially affect the final results. Even in the case of spun bonded webs, when the speed of the conveyor belt is increased, noticeable anisotropy is observed along the direction in which the conveyor travels (machine direction). Thus, we considered fiberwebs with different overall fiber orienta-

(a)

(b)

FIG. 10. (Color online) A web compressed using constant bending step and constant bending span with $T_f = 1/3$ (a) and $T_f = 1/8$ (b).
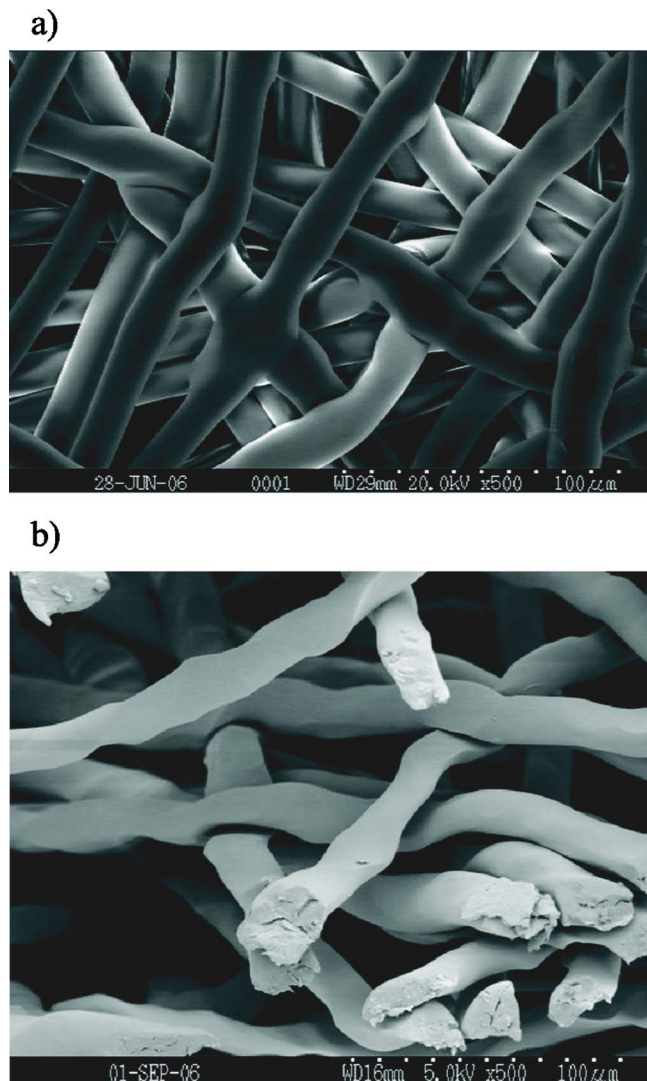

FIG. 9. (Color online) Fiber bending with constant bending step (a) and constant bending span (b) with $T_f = 1/3$.

a)

b)

FIG. 11. (Color online) SEM images of a spun bonded fabric after calendering: (a) top view and (b) side view.

tions in the x and y (machine and cross-machine directions). To generate a fiberweb with fibers highly oriented in the x direction, for instance, fibers were generated randomly as before but with only 10% chance of being the x direction (10% XD), for instance. Five different uncompressed webs having fibers with 10%, 20%, 30%, 40%, and 50% chances of being the y direction are generated. Fiber orientation influences the way fibers will be stacked up. When fibers are mostly deposited in the x direction, for example, a higher number of fibers can be placed in the same plane of constant height (z). Therefore, highly oriented uncompressed webs will have a lower thickness and, consequently, a higher SVF than the isotropic webs. Figure 6 shows the average SVF of the above-mentioned structures versus the percentage of the fibers oriented in the x direction.

As mentioned before another controlling parameter that is used in this work is the minimum allowable distance between parallel fibers at a constant height (z). Figure 7 shows the influence of the gap g on the SVF for a 50×50 web having a dimensionless basis weight of 20. Obviously, increasing g increases the likelihood of having only one fiber at a given height. Increasing g prevents the fibers from depositing in the same altitude and therefore causes the web's thickness to increase almost linearly proportional to the number of deposited fibers and consequently leads to a sharp decrease in the SVF of the media.

III. MODELING COMPRESSION

A. Algorithm

The compression process in this paper is purely geometrical. The fibers on the outside of the web are pushed toward the inside, bending and moving the fibers in their way. Modeling bending of the fibers at the crossovers is complicated and inspired here by the algorithm developed by Niskanen and Alava[3] for simulating wood fibers in paper boards. When fibers are under compression, they bend according to a parameter T_f (see Fig. 8). T_f is the step or slope of the bend, whereas $1/T_f$ is the distance over which each side of a fiber will bend. A large T_f resembles bending of a soft and flexible fiber whereas a small T_f represents rigid fibers. At first glance, and according to Fig. 8, considering T_f or $1/T_f$ constant might seem equivalent. However, this is not true in more complex situations like the one illustrated in Fig. 9. In Fig. 9(a), we assumed a constant step (T_f) during the fiber bending. When fiber A is pushed down against fiber B and bending step $T_f = 1/3$ is kept constant, the cube in fiber C which is in contact with fiber B (i.e., cube number 4, denoted C_4) moves down only by 1/3 (shown by an arrow) and no other cube in fiber C needs to be affected. The alternative scenario is the case where bending distance ($1/T_f$) is kept constant. In this case every time a cube is moved, the bending will be propagated and shared by $1/T_f$ number of cubes on the same fiber. As it can be seen in Fig. 9(b), when C_4 is moved down by 1/3, C_3 and C_2 are also moved each by 1/9 so that a $1/T_f = 3$ total number of cubes are affected. The difference between these two bending models is more evident when T_f is increased. Therefore, the simulation had to be able to handle both scenarios and the differences both in algorithm and results will be presented.

Compression takes place progressively and alternatively from the bottom and the top. The compaction process progresses stepwise and in the unit of fiber diameter (cube side). At each step, the bending procedure will be applied to all the fibers that are affected by the downward (or upward) displacement of the upper (or lower) fibers. The simulation procedure is highly recursive, propagating the compression in breadth, along the fibers, and in depth through contact points. Figures 10(a) and 10(b) show the same fiberweb when compacted from the top and bottom using the above constant-slope and constant-span algorithms with $1/T_f = 3$ and $1/T_f = 8$. Note the flat surface on the top and bottom. It can be seen that the bending of the fibers becomes smoother when the bending slope is reduced. For a realistic simulation, the bending slope should be adjusted according to the mechanical properties of the fibers. Note that our current model is purely geometrical. Relating the T_f parameter to real physical/mechanical properties of a fiberweb is a very inter-
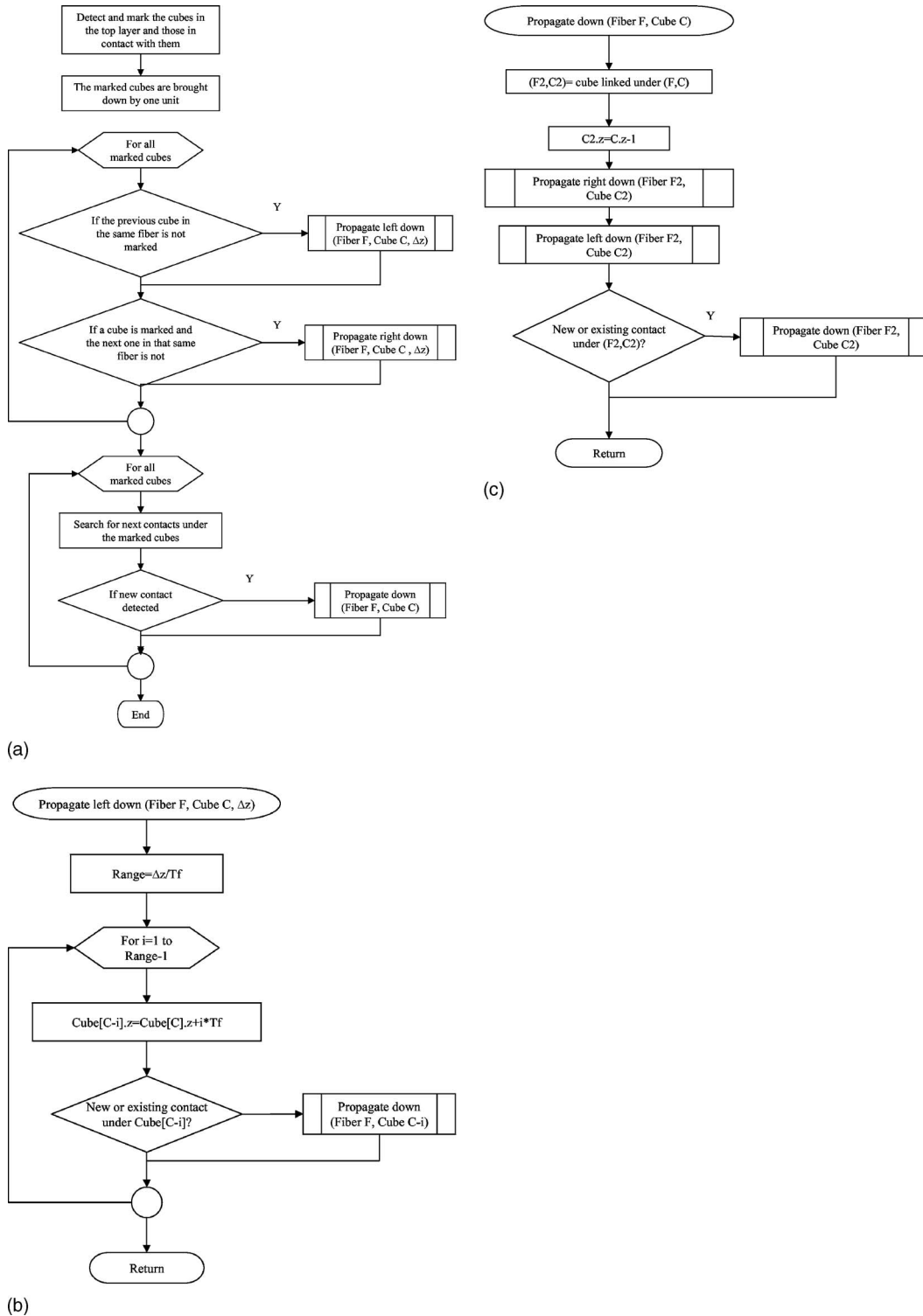
FIG. 12. The flowcharts of the algorithms developed for reducing the web thickness with a constant T_f (a), bending (b), and positioning of the cubes (c).

esting and important step forward. Our geometric model serves as a first step in developing a physical/mechanical model for fiberwebs under compression.

Figure 11 shows two scanning electron microscopy (SEM) images of a spun bonded fabric made of polypropylene fibers with an average diameter of 15 μm after calendering by smooth hot rolls. The spun bonded fibers were produced and calendered in the pilot laboratory of the Nonwovens Cooperative Research Center (NCRC) at NC State

University. Note the similarities between the way fibers bend at the crossovers in Fig. 11(b) and our model shown in Figs. 8–10. Note also that the model does not take into account the flattening of the fibers at the crossovers: the cross section remains a square.

The flowchart in Fig. 12(a) shows the algorithm for reducing the web thickness by one unit when T_f is kept constant. It calls three different subroutines: bend_left_side_down, bend_right_side_down, and propagate

FIG. 14. (Color online) Influence of the calendering temperature and pressure on the SVF of spun bonded fabrics.

The principle remains the same if $1/T_f$ is kept constant, the only difference being in how the bending is calculated in bend_left_down and bend_right_down.

Additional information needs to be stored in the cube structure in order to keep track of which direction they are pushed in and whether or not they are locked in place. In the case of T_f constant, the simulation will attempt to repeat the compression process until a target thickness is reached but if a cube, while moving in one direction, hits or comes in contact with another cube that came from the other direction, the process will be stopped prematurely in order to preserve the slope constant. The case of $1/T_f$ constant does not have this limitation.

B. Compaction ratio

As mentioned before, our algorithm allows a fiberweb to be compressed down to different thicknesses. To demonstrate this, five uncompressed samples were generated according to the aforementioned algorithm (see Sec. II). These structures were made up of 100 fibers with a length of 40 units, laid down randomly in the x or y direction. The thickness of these structures, being statistically a function of the fiber deposition procedure, happened to vary between 43 and 50 units. These structures were compressed to different final thicknesses of 25, 17, 13, 10, and 8 units. Increasing the compaction ratio C_r causes the SVF of the calendered media to increase. Figure 13 shows an uncompressed structure compacted to different thicknesses. It can be seen that by increasing the compaction ratio from 1 to 5, the SVF increases from 4.5% to 25%.

As mentioned before, we also produced spun bonded fabrics made of polypropylene fibers with an average diameter of 15 μm with different basis weights ranging from 20 to 100 g/m^2. These fabrics were compacted using heated smooth calender rolls in NCRC's pilot nonwoven laboratory. Three different temperatures of 105, 120, and 135 °C and three different nip pressures of 200, 400, and 600 lb per linear inch were considered in the experiments. Note that nip pressure is normally shown in force per unit length of the line of contact between the rolls, i.e., width. The influence of the calendering temperature and pressure is shown in Fig. 14 where a given fabric has been calendered under different
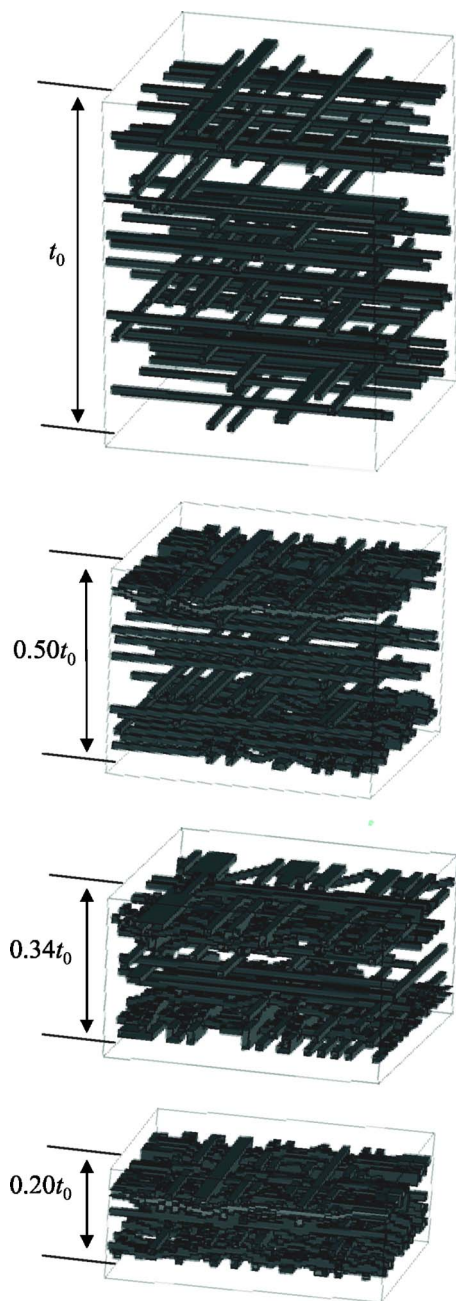

FIG. 13. (Color online) A fluffy structure compacted with different compaction ratios. From top to bottom: (SVF=4.5% and C_r=1.0), (SVF=10% and C_r=2.0), (SVF=15% and C_r=2.9), and (SVF=25% and C_r=5.0). It can be seen that by increasing the compaction ratio from 1 to 5, SVF increases from 4.5% to 25%.

_down. The first two [see Fig. 12(b)] are essentially similar as they take care of bending a fiber in accordance with the T_f parameter, one for each side of the cube along the fiber. When bending, as cubes are lowered, care must be taken to also check for the creation of new contacts. If such contacts are detected, or if the cube being lowered was already in contact with a fiber, a call to propagate_down [see Fig. 12(c)] is made. propagate_down takes care of correctly positioning the cube in contact with the cube calling it and then calls bend_left_down and bend_right_down in order to bend that fiber.
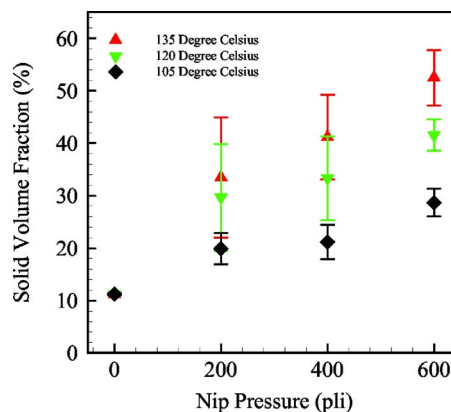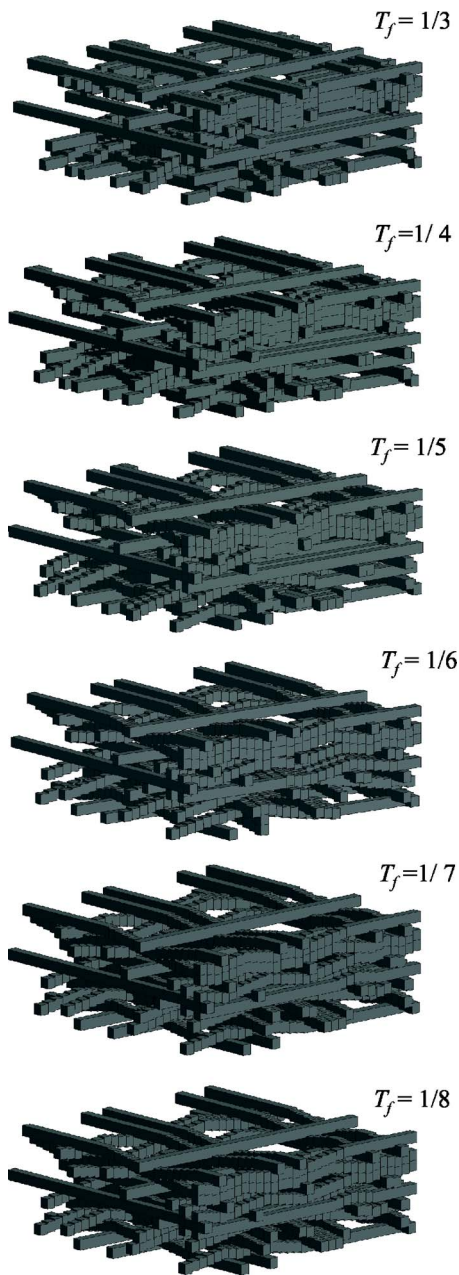
FIG. 15. (Color online) A fiberweb compressed with different bending slopes varying from $T_f = 1/3$ to $T_f = 1/8$.
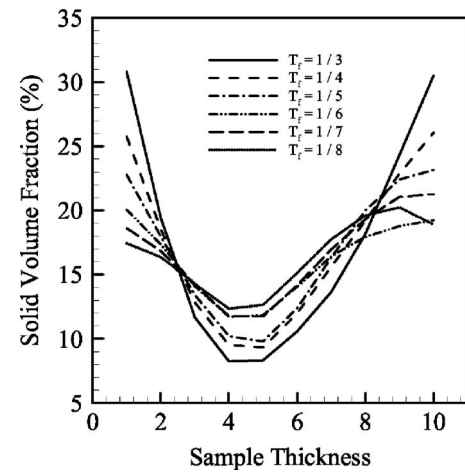

FIG. 16. SVF profiles of the structures shown in Fig. 15. The local SVF is always higher at the top and bottom layers. The higher the bending slope, the greater is the difference between the fabrics' SVF at the outer and inner layers.

the thickness of the incoming fabric, adjusts the gap between the two rolls in such a way that the given nip pressure is achieved. Therefore, no matter what the thickness, all the fabrics are compacted with the same compaction ratio and will have an identical SVF.

C. Effects of fiber rigidity

To study the influence of fiber rigidity on the fabric's permeability, an uncompressed structure was considered and compacted to a final thickness with six different fiber bending slopes (see Fig. 15). As mentioned before, small bending slopes represent rigid fibers whereas large bending slopes model soft and flexible fibers. We used an uncompressed structure with a size of 30×30 made of 50 fibers. This sample had an initial thickness of 25 and an initial SVF of 6.67%. The sample was then compressed to a thickness of 10 units resulting in a SVF of 16.67% using six different bending slopes of $T_f = 1/3 - 1/8$. Figure 16 shows the SVF profile of these structures. It can be seen that the local SVF is always higher at the upper and lower layers as explained before (see Fig. 17). Note that the higher the bending slope (the softer the fiber), the greater is the difference between the SVF at the outer and inner layers. This means that the compression process propagates deeper into the media when the
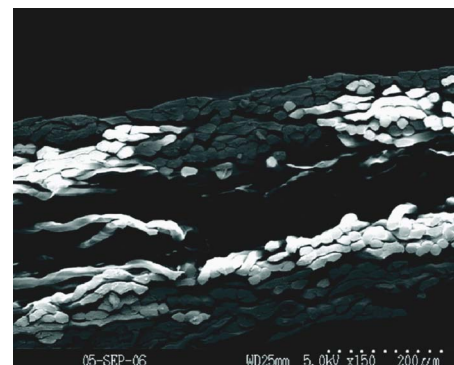
conditions. It can be seen that by increasing the nip pressure, the SVF of the fabric increases. It also shows that increasing the roll temperature leads to an increase in the SVF. Changing the roll temperature and pressure here was only a means of increasing the SVF of the nonwoven media. The data shown in Fig. 14 are averaged over all the basis weights considered. This is because, as discussed in Sec. II, the SVF of a nonwoven fabric is independent of its basis weight. This is also confirmed experimentally in our preliminary experiments (not shown). It is worth mentioning that a similar argument is valid even if the fabrics have been calendered. If the calender's settings are fixed, no matter what the basis weight (thickness), the resulting fabrics will have, within some statistical error, an identical SVF. This is because in a typical calender, a feedback control system, depending on

FIG. 17. (Color online) SEM image of the cross section of a fabric after calendering.
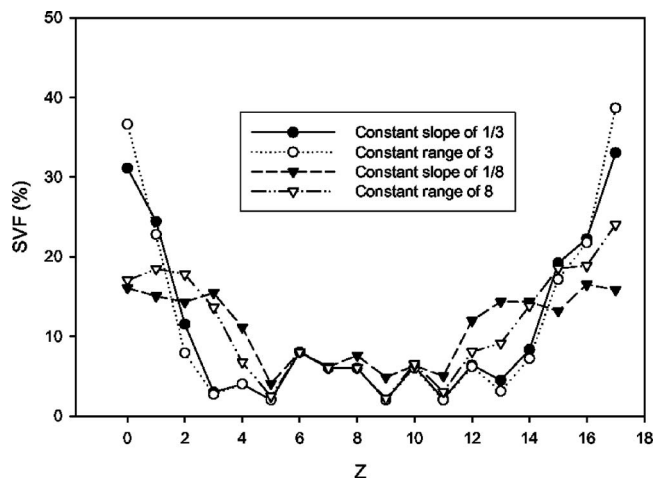
FIG. 18. SVF profile through the thickness of the medium (z). Compaction is based on constant slope and constant span.

fibers are rigid. In other words, high fiber rigidity results in achieving a more uniform SVF across the thickness of the fabric. When the fibers are soft, the SVF increases locally at the outer layers and the middle parts stay very porous. As long as the initial web is the same, the SVF is independent of the value of T_f and of whether T_f or $1/T_f$ is kept constant. However, the profile of the SVF along the thickness of the web is different, as shown in Fig. 18.

IV. MODELING TRANSPORT PHENOMENA

Nonwoven materials have their greatest applications in areas where their interaction with a fluid becomes important. Air and liquid filters, wipes, barrier fabrics, protective clothing, heat and sound insulation materials are among the applications where nonwoven materials are highly demanded. Modeling such properties requires realistic and detailed information of the medium. The simulation algorithm discussed in this paper can serve as a platform for future studies in the above-mentioned areas.[13–15]

V. CONCLUSIONS

In this paper, for the first time, an attempt has been made to model a fiberweb and its structural changes during the thermal calendering process. To simplify this highly complex problem, several assumptions were made. Fibers were assumed to have square cross sections and bend over each other according to a simple set of geometrical rules. The fiber lateral displacement during the compaction process, requiring a series of force balance calculations over the fibers, was ignored as the current algorithm is only designed to model the geometry of a calendered fabric. The fiber orientation is restricted to two directions. The current study is a first step in developing more sophisticated algorithms. Nevertheless, simulation results are in good agreement with our experimental observations. Our results indicate that the calendering has a very significant influence on the fabric's SVF. By calculating the SVF across the fabric's thickness, we obtained a U-shaped profile indicating that the compaction is maximum at the outer layers and minimum in the middle. We have also experimentally observed such a U-shaped SVF profile. The geometries developed here can be used for studying heat and fluid flow through calendered nonwoven fabrics at different levels of compaction.

[1] D. Qi and T. Uesaka, Proceedings of the 1995 International Paper Physics Conference, Niagara-on-the-Lake, Canada, 11–14 September, 1995, p. 65.
[2] A. Koponen, D. Kandhai, E. Hellen, M. Alava, A. Hoekstra, M. Kataja, K. Niskanen, P. Sloot, and J. Timonen, Phys. Rev. Lett. **80**, 716 (1998).
[3] K. Niskanen and M. Alava, Phys. Rev. Lett. **73**, 3475 (1994).
[4] D. S. Clague and R. J. Phillips, Phys. Fluids **9**, 1562 (1997).
[5] M. M. Tomadakis and T. J. Robertson, J. Compos. Mater. **39**, 163 (2005).
[6] M. Kellomaki, J. Astrom, and J. Timonen, Phys. Rev. Lett. **77**, 2730 (1996).
[7] J. Astrom, J. P. Makinen, H. Hirvonen, and J. Timonen, J. Appl. Phys. **88**, 5056 (2000).
[8] X.-F. Wu and Y. A. Dzenis, J. Appl. Phys. **98**, 093501 (2005).
[9] G. G. Chase, V. Beniwal, and C. Venkataraman, Chem. Eng. Sci. **55**, 2151 (2000).
[10] M. T. Senoguz, F. D. Dungan, A. M. Sastry, and J. T. Klamo, J. Compos. Mater. **35**, 1285 (2001).
[11] B. Pourdeyhimi, R. Ramanathan, and R. Dent, Text. Res. J. **66**, 713 (1996).
[12] B. Pourdeyhimi, R. Ramanathan, and R. Dent, Text. Res. J. **66**, 747 (1996).
[13] B. Maze, H. Vahedi Tafreshi, Q. Wang, and B. Pourdeyhimi, J. Aerosol Sci. **38**, 550 (2007).
[14] Q. Wang, B. Maze, H. Vahedi Tafreshi, and B. Pourdeyhimi, Chem. Eng. Sci. **61**, 4871 (2006).
[15] S. Zobel, B. Maze, H. Vahedi Tafreshi, Q. Wang, and B. Pourdeyhimi, "Simulating permeability of 3-D calendered fibrous structures," Chem. Eng. Sci. **62**, 6285–6296 (2007).